

Micromechanics of sheared granular layers activated by fluid pressurization

Hien Nho Gia Nguyen¹, Luc Scholtès^{1,2}, Yves Guglielmi³, Frédéric Victor Donzé⁴, Zady Ouraga⁵, Mountaka Souley⁵

¹Université de Lorraine, CNRS, GeoRessources, Nancy, France

²Université Clermont Auvergne, CNRS, IRD, OPGC, Laboratoire Magmas et Volcans, Clermont-Ferrand, France

³Lawrence Berkeley National Laboratory, Energy Geosciences Division, Berkeley, CA, USA

⁴Université Grenoble-Alpes, CNRS, ISTerre, Grenoble, France

⁵Ineris, Verneuil-en-Halatte, France

Key Points:

- fluid induced reactivation can be either stable or unstable depending on the deformation mode
- slow steady creep is accomodated through distibuted bulk deformation at sub-critical stress states
- accelerated dynamic slip results from intense grain rearrangements localized within the shear band

Corresponding author: Hien Nho Gia Nguyen, nngiahien@gmail.com

Abstract

Fluid pressurization of critically stressed sheared zones can trigger slip mechanisms at work in many geological processes. Using discrete element modeling, we simulate pore-pressure-step creep test experiments on a sheared granular layer under a sub-critical stress state to investigate the micromechanical processes at stake during fluid induced reactivation. The global response is consistent with available experiments and confirms the scale independent nature of fluid induced slip. The progressive increase of pore pressure promotes slow steady creep at sub-critical stress states, and fast accelerated dynamic slip once the critical strength is overcome. Our multi-scale analyses show that these two emergent behaviors correlate to characteristic deformation modes: diffuse deformation during creep, and highly localized deformation during rupture. Creep corresponds to bulk deformation while rupture results from grain rotations initiating from overpressure induced unlocking of contacts located within the shear band which, consequently, acts as a roller bearing for the surrounding bulk.

Plain Language Summary

Fluids can be at the origin of catastrophic disasters, *e.g.*, earthquakes related to deep subsurface fluid injections or landslides triggered by short-term changes of hydrological conditions. It is now well assumed that these phenomena originate from mechanisms taking place in critically stressed shear zones found along tectonic faults, rock mass fractures or localized deformation bands. The increase of pore pressure promotes slip along these shear zones as confirmed by numerous experimental and numerical studies. In this work, we present computer simulations that reproduce the progressive reactivation of a granular shear zone as a result of fluid pressurization. Our simulations provide grain-scale information that improves understanding of fluid induced slip behaviors and illuminate micromechanical details of phenomenological, macroscale observations.

1 Introduction

Fluid overpressurization is one of the primary mechanisms at the origin of tectonic faults slip (Guglielmi et al., 2015; Cappa et al., 2019), giant landslides evolution (Cappa et al., 2014; Agliardi et al., 2020), or even glaciers deformation (Mathews, 1964; Boulton & Hindmarsh, 1987). In all cases, slip results from mechanisms taking place within localized shear zones where most of the stress is accommodated, and it is now well assumed that these mechanisms are very sensitive to variation of pore pressure due to hydrological forcing, related to either natural or anthropogenic processes. Shear zones in tectonically active faults, at the base of large creeping landslides, or in subglacial beds, are generally sub-critically stressed (*i.e.*, subjected to stress condition slightly lower than their instantaneous strength), and their behavior is directly related to stress related perturbations. Fluid induced reactivation can be interpreted in such a context by considering the effective stress principle combined with Mohr-Coulomb (MC) theory (King Hubbert & Rubey, 1959). Pore fluid pressure variations modify the stress state within the shear zone by reducing the effective normal stress while the shear stress remains constant. Following MC theory and assuming that the strength of the shear zone is known (defined through its cohesion c and friction coefficient μ), the critical stress state τ_c at which failure will occur as a result of fluid pressurization is defined by the following criterion:

$$\tau_c = c + \mu(\sigma_N - P) \quad (1)$$

where σ_N is the normal stress acting on the shear zone and P is the pore fluid pressure.

Nonetheless, the MC criterion does not give any information on the mechanisms developing before or after failure. This is rather limiting since shear zones can promote different modes of slip, stable or unstable, sometimes even before the critical stress state is reached (Guglielmi et al., 2015; Scuderi & Collettini, 2016; Scuderi et al., 2017; Cappa

et al., 2019). The rate- and state- friction (RSF) theory offers a sound and well established framework to characterize slip behaviors (Dieterich, 1979; Ruina, 1983; Aharonov & Scholz, 2018). However, even with modifications specifically dedicated to fluid pressure perturbations (Linker & Dieterich, 1992), the RSF theory seems in contradiction with certain behaviors observed in nature (Cappa et al., 2019) or in laboratory (Scuderi et al., 2017). In short, fluid assisted fault reactivation and earthquake triggering cannot be explained in the context of frictional stability analysis for which an increase of fluid pressure should favor stable aseismic slip (Segall & Rice, 1995; Scholz, 1998).

It is now well assumed that shear zones may accumulate displacement in two ways, through either stable creep, or dynamic rupture (Dieterich, 1979; Ruina, 1983). These 2 deformation modes are incidentally related respectively to the aseismic and seismic behaviors used to characterize tectonic faults slip (Reinen, 2000), which have been both observed as a result of fluid pressurization (Cornet et al., 1998). Nonetheless, despite the compelling evidence of slip phenomena caused by pore pressure perturbations, the mechanisms at play remain poorly understood (Scuderi et al., 2017; Scuderi & Collettini, 2018). Indeed, shear zones are more complex than single sliding surface systems. They are generally filled with layers of particulate materials which are commonly termed "gouges" in the tectonic context. The response of such materials to stress perturbations results from frictional sliding, rolling, breaking and rearrangement of grains which are undoubtedly more intricate in the presence of hydromechanical processes.

In this paper, we propose to relate the macroscopic response of a granular shear zone to the micromechanical phenomena at work during fluid induced reactivation. For that matter, we developed a numerical experiment inspired by the experiments performed in (Scuderi et al., 2017) where a sub-critically stressed granular layer is subjected to a progressive pore pressure increase. The numerical experiment is built upon a numerical model based on the discrete element method (DEM) which offers a unique approach to simulate complex emergent behaviors by treating the medium under consideration as an assembly of individual particles interacting one with another according to simplified contact laws (Cundall & Strack, 1979). DEM models have proven effective in producing emergent behaviors representative of fault gouges dynamics for several decades now (Morgan & Boettcher, 1999; Aharonov & Sparks, 2004; Ferdowsi et al., 2013; Ferdowsi & Rubin, 2020). Recent efforts have actually illustrated their capability to investigate friction related fluid coupled processes (Dorostkar et al., 2017; Yang & Juanes, 2018). In this study, we use a hydromechanically coupled DEM model to simulate fluid induced reactivation of a sub-critically stressed shear zone, so as to highlight the micromechanical processes at the origin of the different macroscopic slip behaviors observed.

2 Method

To investigate fluid induced reactivation of sheared granular layers, we utilized a discrete element model coupled with a pore-scale finite volume (PFV) scheme implemented in the YADE DEM software (Šmilauer et al., 2010). The numerical medium consists of a 3D polydisperse assembly of 12,000 spherical particles with a uniform size distribution such that their diameters vary between 0.066mm and 0.133mm. The assembly is enclosed in between two rigid walls in the y direction, and periodic boundaries are defined in both the x and z directions such that particles exit from one side and reappear on the other (Figure 1(a)). This configuration enables to simulate an infinite and homogeneous horizontal layer with a limited computational cost without sacrificing potentially important out of plane particle reorganizations which can be of significance in terms of emerging behaviors (Hazzard & Mair, 2003). Particles interact one with another through elastic-frictional interactions. Each particle is identified by its own mass, radius and moment of inertia. An explicit solution scheme is used to integrate Newton's second law so as to update the particles' positions according to the forces they are subjected to. Compressible fluid flow is modeled within the pore space which is discretized based on a regular

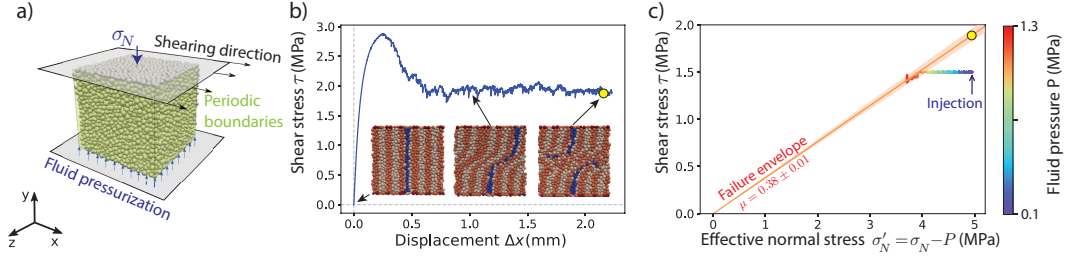


Figure 1. Numerical experiment. (a) DEM model set-up: geometry and boundary conditions defining the granular shear zone. (b) Preconditioning stage: direct shear test to localize shear within the layer. Once the steady-state strength is reached, the shear stress is reduced to 80% of its value prior to fluid injection. (c) Pore-pressure-step creep test: pore fluid pressure is progressively increased under constant shear stress so that the normal effective stress decreases up to failure. The Mohr-Coulomb criterion is plotted for reference.

101 Delaunay triangulation of the particles' centers (see (Chareyre et al., 2012; Catalano et
 102 al., 2014; Scholtès et al., 2015) for details of the implementation). The method is hydro-
 103 mechanically coupled in the sense that deformation of the pore space caused by partic-
 104 les' movements induces pore pressure variations and associated interporal flow, while
 105 pore pressure changes induce hydraulic forces on the solid particles and associated stress
 106 variations. For this study, we considered fluid properties representative of water, with
 107 a bulk modulus of 2.2 GPa and a viscosity of 1 mPa.s. The model's parameters and the
 108 emergent properties of the simulated shear zone are provided in the supplementary file
 109 (Table 1).

110 The numerical sample is prepared by first hydrostatically compacting a cloud of
 111 randomly positioned particles up to 1 MPa (we don't consider gravitational forces in our
 112 simulation). The sample is then subjected to a normal stress σ_N of 5 MPa in the y di-
 113 rection through the displacement of the top and bottom walls (the walls are frictionless
 114 during this stage). Once equilibrium is reached, the particles in contact with the walls
 115 are glued to them in order to produce a certain degree of roughness at the interfaces. The
 116 top wall is then translated at a constant displacement rate of $2 \times 10^{-5} \text{ m s}^{-1}$ while the
 117 bottom wall is fixed to reach a steady-state strength (Figure 1(b)). This precondition-
 118 ing stage ensures shear to localize within the simulated medium in the form of a shear
 119 band with a thickness of approximately 10 particles, as commonly observed in granu-
 120 lar materials (Rattez et al., 2020). Once steady state strength and shear localization are
 121 ensured, the top wall is stopped and the control mode changes from displacement-controlled
 122 to stress-controlled. Similarly to the creep experiments performed by Scuderi et al. (Scuderi
 123 et al., 2017), the shear stress τ is reduced to 80% of the steady state strength τ_{ss} and
 124 then kept constant at this sub-critical level while the pore fluid pressure P is increased
 125 stepwise to simulate a progressive reduction of the effective normal stress $\sigma'_N = \sigma_N -$
 126 P (Figure 1(c)). One has to note that the preconditioning stage is controlled to ensure
 127 a quasi-static response of the system (the inertial number $I = \frac{\dot{\gamma} D_p}{P/\rho}$ is equal to $2.045 \times$
 128 10^{-7} (MiDi, 2004)). The creep test being stress-controlled, the system response is di-
 129 rectly related to the layer's dynamics (no numerical damping is used during this stage).

130 3 Macroscopic behaviors

131 The simulated emergent behavior show strong similarities with slip behaviors ob-
 132 served in laboratory (Scuderi et al., 2017; Scuderi & Collettini, 2018; Agliardi et al., 2020)
 133 and in situ (Guglielmi et al., 2015; Cappa et al., 2019) experiments under similar con-

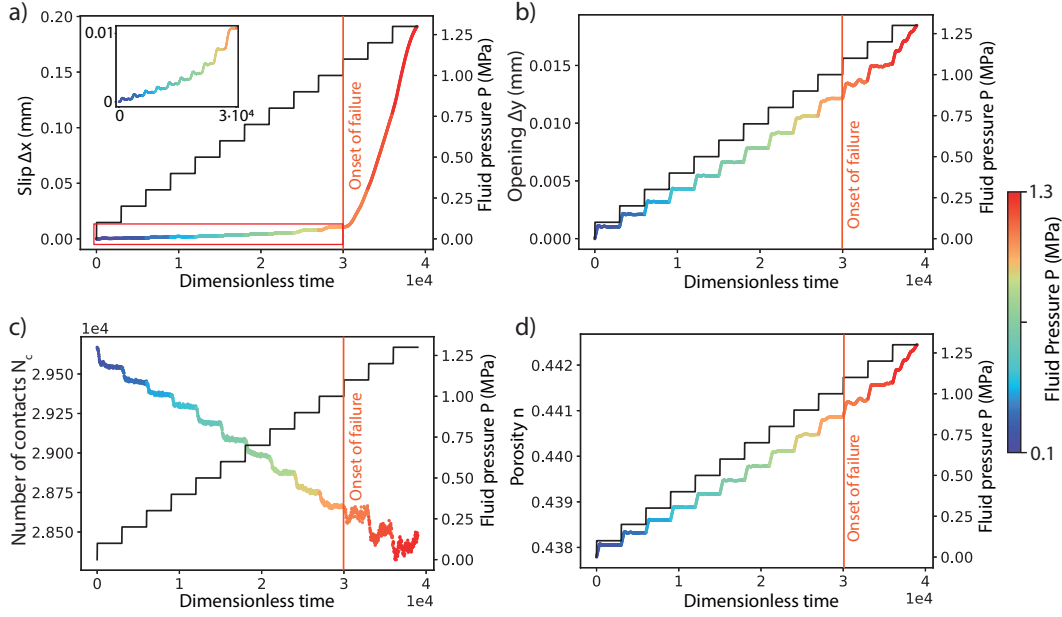


Figure 2. Response of the simulated shear zone during progressive fluid pressurization. (a) Shear displacement with a zoom up to the pre-failure state. (b) Normal displacement. (c) Total number of sphere-sphere contacts. (d) Evolution of the porosity. The curves are color-coded as functions of the fluid pressure P . Fluid pressure curves are plotted in black in each graph for reference.

134 conditions: slow steady slip is first observed up to the critical stress state ($\mu\sigma'_N \approx \tau_{ss}$) from
 135 which accelerated slip is then triggered. Those two stages have been assimilated by Scuderi
 136 et al. (Scuderi et al., 2017) respectively to the steady-state and unstable creep behav-
 137 iors observed during secondary and tertiary creeps of intact rock (Brantut et al., 2013).
 138 Our simulation does not show any evidence of primary creep related compaction during
 139 the preconditioning stage of the loading as observed in (Scuderi et al., 2017). The
 140 compaction is most certainly related to time-dependent processes (*e.g.*, pressure solu-
 141 tion) leading to grain to grain indentation that we did not take into account in our model
 142 formulation.

143 The first stage is characterized by a quasi-linear increase of both the shear and normal
 144 displacements as functions of the fluid pressure increase. Each pressure step pro-
 145 duces an almost instantaneous acceleration of the system before it stabilizes to a new
 146 steady state (characterized by the successive plateaux on the curves). The amplitudes
 147 of the normal displacement steps remain proportional to the pressure increase over the
 148 entire stage (Figures 2(b)), while the amplitudes of the shear displacement steps tends
 149 to slightly increase as the system approaches the critical stress state (Figures 2(a)). Sim-
 150 ilarly to what was observed in the experiments of Scuderi et al. (Scuderi et al., 2017),
 151 the layer suffers a systematic overall dilation resulting from the fluid pressurization. The
 152 volumetric deformation of our numerical shear zone directly correlates to its opening and
 153 is proportional to the pressure increase (Figure 2(d)). This pressure induced dilation causes
 154 a progressive loss of interparticle contacts also proportional to the pressure increase, sug-
 155 gesting a redistribution of some interparticle forces into hydrostatic forces (Figure 2(c)).

156 The second stage is characterized by a rapid acceleration of slip that spontaneously
 157 evolves into dynamic failure as suggested by the slight decrease of shear stress described
 158 by the red portion of the curve in Figure 1(c). In agreement with the experiment done

159 by Scuderi et al. (Scuderi et al., 2017), the onset of failure corresponds almost exactly
 160 to the moment where the stress state approaches the critical stress state (the Mohr-Coulomb
 161 criterion). In contradiction to what was observed in the laboratory, the medium contin-
 162 uously dilates at a quasi-constant rate during this accelerated slip phase with, nonethe-
 163 less, a slight acceleration after significant slip has developed (visible at the last pressure
 164 step, where P increases from 1.2 MPa to 1.3 MPa on Figure 2(b)). The lack of compaction
 165 during this accelerated slip stage is most certainly related to the fact that grain crush-
 166 ing is not possible in our numerical model while cataclasis and grain size reduction were
 167 systematically observed in the experiments. The oscillations in the evolution of both the
 168 opening and the number of contacts illustrate the dynamic and unstable nature of the
 169 response. The amplitudes of these oscillations are more pronounced than during the slow
 170 steady slip stage and suggest intense grains rearrangements within the medium.

171 We can summarize our results by saying that fluid pressurization induces slip well
 172 before reaching the critical steady-state strength. Slip remains slow and steady as long
 173 as this critical state is not reached. It accelerates to failure afterward, with some insta-
 174 bilities emerging from grain scale rearrangements. Dilation persists during the entire fluid
 175 pressurization and appears to develop at a quasi-constant rate, directly proportional to
 176 the pressure increase, whatever the emergent slip behavior.

177 The hydro-mechanical behaviors predicted by our numerical shear zone shows great
 178 similarities with behaviors observed both in laboratory and in situ on shear zones pre-
 179 senting different natures and subjected to different stress states (Guglielmi et al., 2015;
 180 Scuderi et al., 2017; Scuderi & Collettini, 2018; Cappa et al., 2019; Agliardi et al., 2020).
 181 Besides the relevance of the method itself and the confirmation that our DEM model con-
 182 stitutes a good analogue to study natural shear zones, our results confirm the consistency
 183 of shear zones' response to short term pore pressure variations despite the scale effect
 184 and the added complexity of natural environments.

185 4 Micromechanical processes

186 In order to get further insights into the mechanisms at work at the grain scale, we
 187 discretized the shear zone into 12 equal-sized sub-layers parallel to the shearing direc-
 188 tion to estimate the vertical distributions of the quantities presented in Figure 2. Each
 189 layer is approximately 3 particles thick. The pressurization induced variations of slip,
 190 opening, number of contacts and porosity are presented in Figure 3 as vertical profiles
 191 corresponding respectively to 2 pre-failure states and 2 post-failure states (onset of fail-
 192 ure occurs when the fluid pressure P increases from 1 MPa to 1.1 MPa).

193 In terms of displacements (Figures 3(a,b)), shear is preferentially localized within
 194 the shear band after failure. The profiles at sub-critical states ($P=0.7$ and 0.9 MPa) show
 195 slight but limited S-bend shapes compared to the post-failure states. The S-bend shape
 196 highlights the role of the shear band on the overall response and the relative passiveness
 197 of the surrounding bulk with regards to slip. A similar but less pronounced trend can
 198 be observed for the opening displacement profiles where inflexion points can be noticed
 199 at the shear band's boundaries. As observed macroscopically in Figures 2(a,b), the open-
 200 ing increments scale almost proportionally with the pore pressure increment at all stages,
 201 in contrast with the exponential increase of the post-failure slip increments.

202 The variations of the number of contacts and porosity (Figures 3(cd)) clearly point
 203 out to 2 different mechanisms representative respectively of (i) the slow and steady pre-
 204 failure creep, and (ii) the accelerated and dynamic post-failure slip. Both quantities evolve
 205 quasi-monotonically before failure across the entire layer, indicating an homogeneous re-
 206 sponse of the bulk to the pressurization: every increment of pore pressure leads to a loss
 207 of contacts as well as to a porosity increase which, as suggested by the macroscopic re-
 208 sponses (Figures 2(cd)), are almost proportional to the pressure increase. After failure

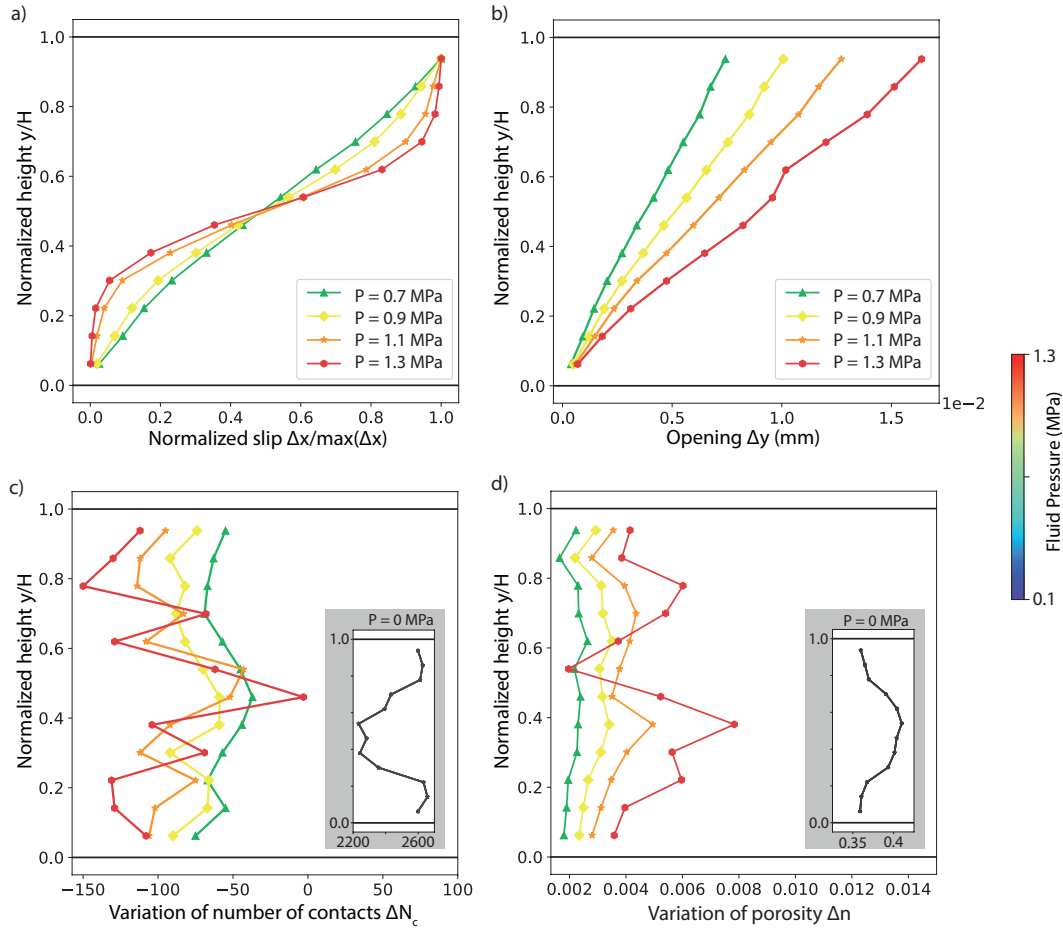


Figure 3. Profiles showing the vertical variation distributions of: (a) normalized slip, (b) opening, (c) number of contacts and (d) porosity within the shear zone at different stages of the fluid pressurization. The curves are color-coded as functions of the fluid pressure. Onset of failure occurs when the fluid pressure P increases from 1 MPa to 1.1 MPa. Inset figures in c) and d) show the vertical distributions of both the number of contacts and the porosity at the initial state, before fluid pressurization ($P=0$).

209 ($P > 1.1$ MPa), both quantities highlight a localization of the deformation inside the shear
 210 band where contacts are gained and porosity decreases as described by the clear mid-
 211 height spike observed at $P = 1.3$ MPa in both profiles. This indicates shear induced com-
 212 paction within the shear band. Interestingly, the evolutions of both quantities outside
 213 the shear band follow the trends observed prior to failure, namely, loss of contacts and
 214 porosity increase. The coexistence of these somewhat opposite volumetric trends in and
 215 out of the shear band suggests deformation mechanisms taking place at the interfaces
 216 between the bulk and the shear band where a large amount of the opening is accommo-
 217 dated as suggested by the 2 spikes in the porosity profile at $P = 1.3$ MPa ($\frac{y}{H} \approx 0.4, 0.8$),
 218 in conjunction with a noticeable gain of contacts below these interfaces ($\frac{y}{H} \approx 0.3, 0.7$).
 219 These post-failure profiles suggest sharply defined sub-horizontal structures that could
 220 actually be assimilated to the so-called Y-shears commonly observed in sheared mate-
 221 rials in natural context (Reinen, 2000) and in experiments, either in the laboratory (Scuderi
 222 & Colletini, 2018) or in numerical analogs (Morgan & Boettcher, 1999).

223 Our observations suggest a high degree of particle rearrangement once accelerated
 224 slip occurs, leading to the generation of a hyperactive layer (the shear band) effectively
 225 disconnected from the surrounding material by discrete structures. By tracking the ro-
 226 tation of particles during the reactivation process (Figure 4(a)), we confirm the micromech-
 227 anisms at play: slow steady creep corresponds to bulk deformation due to interlocked
 228 particles, while accelerated dynamic slip is mainly accommodated by interparticle rolling
 229 concentrated within the shear band. As discussed by Morgan and Boettcher (Morgan
 230 & Boettcher, 1999), shear loads within granular materials are borne by chains of par-
 231 ticles carrying high forces. These chains evolve during shear and eventually fail due to
 232 interparticle rolling. We posit that post-failure accelerated slip is triggered by the sud-
 233 den collapse of these force chains (a mechanism identified as force-chain buckling in the
 234 literature by, *e.g.*, (Tordesillas, 2007)) within the shear band. As shown in Figure 4(b),
 235 the interparticle contact forces align to the direction of the maximum principal stress
 236 for both pre-failure and post-failure states (inclined at approximately 45° to the load-
 237 ing direction). Strong force chains are predominantly located within the shear band be-
 238 fore failure. The same strong force chains actually persist up to failure (Figure 4(b)) and
 239 disappear once failure occurs. Once particles start to roll, the entire shear band acts as
 240 a roller bearing which promotes slip of the surrounding bulk. One can note that the slip
 241 rate tends to stabilize once this roller bearing is activated. Strong interparticle forces still
 242 concentrate within the shear band as a result of its compaction, but in a more diffuse
 243 manner. Interestingly, the distribution of sliding contacts (Figure 4(c)) does not directly
 244 correlate with particle rotations, specially just before the onset of failure ($P = 1$ MPa) where
 245 particles start to slide intensively inside the shear band while interparticle slips were
 246 only scarcely distributed over the entire system at lower pore pressures (*e.g.*, $P = 0.7$ MPa).
 247 These interparticle slips occurring inside the shear band just before the onset of failure
 248 are clear precursors of the force chain collapses that lead to particle rolling and overall
 249 failure. Post-failure, interparticle slips tend to occur mainly inside the shear band where
 250 most particle rearrangements are concentrated, but some particles also slip outside of
 251 the shear band.

252 To sum up, pre-failure slow steady creep is associated to diffuse bulk deformation
 253 while post-failure accelerated dynamic slip results from very localized deformation pro-
 254 cesses taking place within the shear band. Similarly to what was observed in laboratory
 255 experiments on a saturated granular till (Rathbun & Marone, 2010), the pressurization
 256 of the layer induces a progressive transition from distributed shear to localized deforma-
 257 tion. Evidence of this bi-modal accommodation of slip has also been observed in dry ser-
 258 pentinite gouge by Reinen (Reinen, 2000) who concluded that the microstructures that
 259 form during shear may be used to identify the seismic behavior of natural fault zones.
 260 Our numerical results tend to confirm her conclusions stating that stable fault creep re-
 261 sults from distributed deformation, while localized deformation favors unstable dynamic
 262 slip. Before failure, grain reorganizations are very limited and the overall response of the

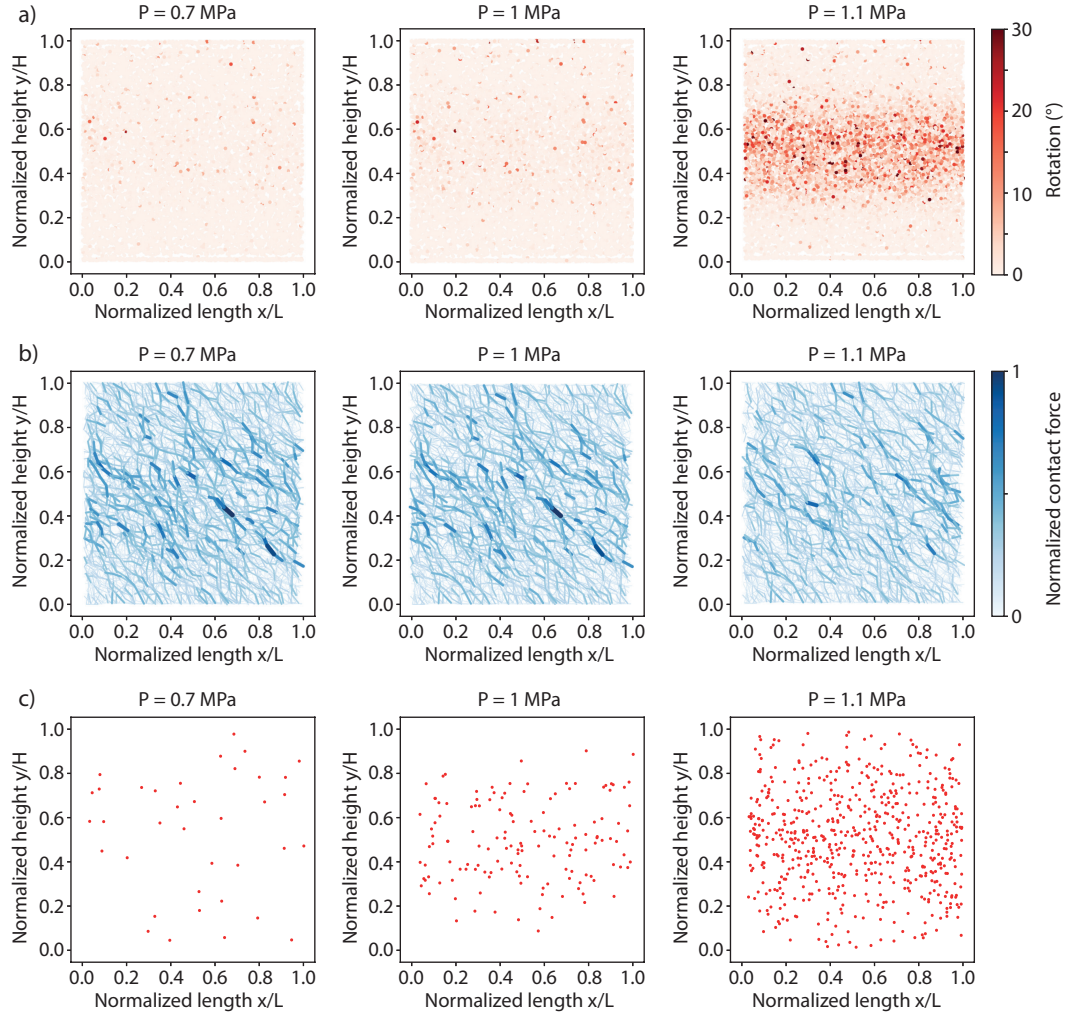


Figure 4. Microscale analyses on a vertical slice extracted from the sample at different stages of the reactivation: $P = 0.7$ MPa, $P = 1$ MPa, and $P = 1.1$ MPa. (a) Spatial distribution maps of accumulated particle rotations. (b) Interparticle contact force network, color intensity and thicknesses of the line segments are proportional to the contact force magnitude. Normalized contact force is computed from all considered stages. (c) Spatial distribution of sliding contacts. Adjacent contacts with the two boundary walls are omitted to focus on what happens within the sample. Onset of failure occurs when the fluid pressure P was increased from 1 MPa to 1.1 MPa.

263 shear zone is driven by bulk deformation. Once failure occurs, the shear band concen-
 264 trates all the grain rearrangements at the origin of the accelerated slip. As suggested by
 265 Morgan and Boettcher (Morgan & Boettcher, 1999), failure is directly correlated to grain
 266 rotations which promotes a dynamic response of the system.

267 5 Concluding remarks

268 We used a discrete element model to analyze the micromechanics of fluid induced
 269 reactivation of a granular shear zone under a sub-critical stress state. We were able to
 270 reproduce typical slip behaviors observed both in laboratory and in situ experiments:
 271 at constant shear stress, fluid pressurization reduces the normal stress and promotes slip
 272 through (i) slow steady slip before the critical state is reached, and (ii) accelerated dy-
 273 namic slip afterward. Our micromechanical analysis show that these two slip behaviors
 274 are directly related to two distinct deformation modes: (i) a distributed mode where the
 275 entire layer deforms homogeneously in response to the pressure increase, and (ii) a lo-
 276 calized mode where the shear band acts as a roller bearing for the surrounding bulk. The
 277 transition between these two deformation modes results from the rupture of interpar-
 278 ticle force chains located within the shear band. By reducing the effective stress, fluid
 279 overpressurization promotes interparticle slips along these force chains which eventually
 280 lead to intense particle rearrangements once the critical stress state is reached. Pre-failure
 281 slip is mainly accomodated by dilation induced elastic shear distributed over the entire
 282 bulk, while post-failure slip is mainly accomodated through particle rolling located within
 283 the shear band. Our results suggest that grain rotations promote slip instabilities dur-
 284 ing fluid pressurization of granular shear zones.

285 Our numerical experiment constitutes a simplification of realistic configurations and
 286 it is evident that the simplicity of such an idealized system affect its mechanical behav-
 287 ior (*e.g.*, the sphericity of particles has a strong influence on the macroscopic volumet-
 288 ric deformations). Nonetheless, several studies have shown that discrete element mod-
 289 els can be considered as a good first approximation to understand the complexity of the
 290 mechanisms that characterize shear zones during deformation (Morgan & Boettcher, 1999;
 291 Aharonov & Sparks, 2004; Mair & Hazzard, 2007; Rathbun et al., 2013). Even though
 292 the present study provides insight into the micromechanisms at work in pressurized gran-
 293 ular shear zones, additional work is needed to fully characterize fluid induced slip be-
 294 haviors in natural shear zones. For instance, beside the influence of key loading param-
 295 eters such as the injection rate or the normal stress that needs to be investigated, the
 296 introduction of time-dependent physics in the model formulation as suggested for exam-
 297 ple by (Van Den Ende et al., 2018) would allow to discuss fluid induced slip behaviors
 298 in the context of the rate- and state- friction theory, while the consideration of crush-
 299 able grains as proposed for example by (Abe & Mair, 2009) would give further insights
 300 into the deformation process since grain fracturing plays a key role in the evolution of
 301 gouge during shear.

302 Acknowledgments

303 This work was supported partly by the french PIA project “Lorraine Université d’Excellence”,
 304 reference ANR-15-IDEX-04-LUE. The source code of the YADE-DEM software used for
 305 the simulations in this study is available at <https://yade-dem.org/doc/installation.html>
 306 (Šmilauer et al., 2010).

307 References

- 308 Abe, S., & Mair, K. (2009). Effects of gouge fragment shape on fault friction: New
 309 3d modelling results. *Geophysical Research Letters*, *36*(23). doi: 10.1029/
 310 2009GL040684

- 311 Agliardi, F., Scuderi, M. M., Fusi, N., & Collettini, C. (2020). Slow-to-fast
312 transition of giant creeping rockslides modulated by undrained loading in
313 basal shear zones. *Nature Communications*, *11*(1), 1352. doi: 10.1038/
314 s41467-020-15093-3
- 315 Aharonov, E., & Scholz, C. H. (2018). A physics-based rock friction constitutive law:
316 Steady state friction. *Journal of Geophysical Research: Solid Earth*, *123*(2),
317 1591-1614. doi: 10.1002/2016JB013829
- 318 Aharonov, E., & Sparks, D. (2004). Stick-slip motion in simulated granular lay-
319 ers. *Journal of Geophysical Research: Solid Earth*, *109*(B9). doi: 10.1029/
320 2003JB002597
- 321 Boulton, G. S., & Hindmarsh, R. C. A. (1987). Sediment deformation beneath
322 glaciers: Rheology and geological consequences. *Journal of Geophysical Re-
323 search: Solid Earth*, *92*(B9), 9059-9082. doi: 10.1029/JB092iB09p09059
- 324 Brantut, N., Heap, M. J., Meredith, P. G., & Baud, P. (2013). Time-dependent
325 cracking and brittle creep in crustal rocks: A review. *Journal of Structural Ge-
326 ology*, *52*, 17-43. doi: 10.1016/j.jsg.2013.03.007
- 327 Cappa, F., Guglielmi, Y., Viseur, S., & Garambois, S. (2014). Deep fluids can fa-
328 cilitate rupture of slow-moving giant landslides as a result of stress transfer
329 and frictional weakening. *Geophysical Research Letters*, *41*(1), 61-66. doi:
330 10.1002/2013GL058566
- 331 Cappa, F., Scuderi, M. M., Collettini, C., Guglielmi, Y., & Avouac, J.-P. (2019).
332 Stabilization of fault slip by fluid injection in the laboratory and in situ. *Sci-
333 ence Advances*, *5*(3), eaau4065.
- 334 Catalano, E., Chareyre, B., & Barthélémy, E. (2014). Pore-scale modeling of fluid-
335 particles interaction and emerging poromechanical effects. *International Jour-
336 nal for Numerical and Analytical Methods in Geomechanics*, *38*(1), 51-71. doi:
337 10.1002/nag.2198
- 338 Chareyre, B., Cortis, A., Catalano, E., & Barthélemy, E. (2012). Pore-Scale Mod-
339 eling of Viscous Flow and Induced Forces in Dense Sphere Packings. *Transport
340 in Porous Media*, *92*(2), 473-493. doi: 10.1007/s11242-011-9915-6
- 341 Cornet, F. H., Helm, J., Poitrenaud, H., & Etchecopar, A. (1998). Seismic and aseis-
342 mic slips induced by large-scale fluid injections. In S. Talebi (Ed.), *Seismicity
343 associated with mines, reservoirs and fluid injections* (p. 563-583). Basel:
344 Birkhäuser Basel.
- 345 Cundall, P. A., & Strack, O. D. L. (1979). A discrete numerical model for granular
346 assemblies. *Géotechnique*, *29*(1), 47-65. doi: 10.1680/geot.1979.29.1.47
- 347 Dieterich, J. H. (1979). Modeling of rock friction: 1. experimental results and consti-
348 tutive equations. *Journal of Geophysical Research: Solid Earth*, *84*(B5), 2161-
349 2168. doi: 10.1029/JB084iB05p02161
- 350 Dorostkar, O., Guyer, R. A., Johnson, P. A., Marone, C., & Carmeliet, J. (2017).
351 On the micromechanics of slip events in sheared, fluid-saturated fault gouge.
352 *Geophysical Research Letters*, *44*(12), 6101-6108. doi: 10.1002/2017GL073768
- 353 Ferdowsi, B., Griffa, M., Guyer, R. A., Johnson, P. A., Marone, C., & Carmeliet, J.
354 (2013). Microslips as precursors of large slip events in the stick-slip dynamics
355 of sheared granular layers: A discrete element model analysis. *Geophysical
356 Research Letters*, *40*(16), 4194-4198. doi: 10.1002/grl.50813
- 357 Ferdowsi, B., & Rubin, A. M. (2020). A granular physics-based view of fault fric-
358 tion experiments. *Journal of Geophysical Research: Solid Earth*, *125*(6),
359 e2019JB019016. doi: 10.1029/2019JB019016
- 360 Guglielmi, Y., Cappa, F., Avouac, J.-P., Henry, P., & Elsworth, D. (2015). Seismic-
361 ity triggered by fluid injection-induced aseismic slip. *Science*, *348*(6240), 1224-
362 1226. doi: 10.1126/science.aab0476
- 363 Hazzard, J. F., & Mair, K. (2003). The importance of the third dimension in granu-
364 lar shear. *Geophysical Research Letters*, *30*(13). doi: 10.1029/2003GL017534
- 365 King Hubbert, M., & Rubey, W. W. (1959). Role of fluid pressure in mechanics of

- 366 overthrust faulting: I. mechanics of fluid-filled porous solids and its application
 367 to overthrust faulting. *Geological Society of America Bulletin*, 70(2), 115-166.
- 368 Linker, M. F., & Dieterich, J. H. (1992). Effects of variable normal stress on rock
 369 friction: Observations and constitutive equations. *Journal of Geophysical Re-*
 370 *search: Solid Earth*, 97(B4), 4923-4940. doi: 10.1029/92JB00017
- 371 Mair, K., & Hazzard, J. F. (2007). Nature of stress accommodation in sheared gran-
 372 ular material: Insights from 3d numerical modeling. *Earth and Planetary Sci-*
 373 *ence Letters*, 259(3), 469-485. doi: 10.1016/j.epsl.2007.05.006
- 374 Mathews, W. H. (1964). Water pressure under a glacier. *Journal of Glaciology*,
 375 5(38), 235-240. doi: 10.3189/S0022143000028811
- 376 MiDi, G. (2004). On dense granular flows. *The European Physical Journal E*, 14,
 377 341-365. doi: 10.1140/epje/i2003-10153-0
- 378 Šmilauer, V., Catalano, E., Chareyre, B., Dorofeenko, S., Duriez, J., Gladky, A., ...
 379 others (2010). Yade reference documentation. *Yade Documentation*, 474(1).
- 380 Morgan, J. K., & Boettcher, M. S. (1999). Numerical simulations of granular shear
 381 zones using the distinct element method: 1. shear zone kinematics and the
 382 micromechanics of localization. *Journal of Geophysical Research: Solid Earth*,
 383 104(B2), 2703-2719. doi: 10.1029/1998JB900056
- 384 Rathbun, A. P., & Marone, C. (2010). Effect of strain localization on frictional be-
 385 havior of sheared granular materials. *Journal of Geophysical Research: Solid*
 386 *Earth*, 115(B1). doi: 10.1029/2009JB006466
- 387 Rathbun, A. P., Renard, F., & Abe, S. (2013). Numerical investigation of the in-
 388 terplay between wall geometry and friction in granular fault gouge. *Journal of*
 389 *Geophysical Research: Solid Earth*, 118(3), 878-896. doi: 10.1002/jgrb.50106
- 390 Rattez, H., Shi, Y., Sac-Morane, A., Klaeyle, T., Mielniczuk, B., & Veveakis, M.
 391 (2020). Effect of grain size distribution on the shear band thickness evolution
 392 in sand. *Géotechnique*, 0(0), 1-39. doi: 10.1680/jgeot.20.P.120
- 393 Reinen, L. A. (2000). Seismic and aseismic slip indicators in serpentinite gouge. *Ge-*
 394 *ology*, 28(2), 135-138. doi: 10.1130/0091-7613(2000)28<135:SAASII>2.0.CO;
 395 2
- 396 Ruina, A. (1983). Slip instability and state variable friction laws. *Jour-*
 397 *nal of Geophysical Research: Solid Earth*, 88(B12), 10359-10370. doi:
 398 10.1029/JB088iB12p10359
- 399 Scholtès, L., Chareyre, B., Michallet, H., Catalano, E., & Marzougui, D. (2015).
 400 Modeling wave-induced pore pressure and effective stress in a granular
 401 seabed. *Continuum Mechanics and Thermodynamics*, 27(1), 305-323. doi:
 402 10.1007/s00161-014-0377-2
- 403 Scholz, C. (1998). Earthquakes and friction laws. *Nature*, 391, 37-42. doi: 10.1038/
 404 34097
- 405 Scuderi, M., & Collettini, C. (2016). The role of fluid pressure in induced vs. trig-
 406 gered seismicity: insights from rock deformation experiments on carbonates.
 407 *Scientific Reports*, 6(24852). doi: 10.1038/srep24852
- 408 Scuderi, M., & Collettini, C. (2018). Fluid Injection and the Mechanics of Fric-
 409 tional Stability of Shale-Bearing Faults. *Journal of Geophysical Research: Solid*
 410 *Earth*, 123(10), 8364-8384. doi: 10.1029/2018JB016084
- 411 Scuderi, M., Collettini, C., & Marone, C. (2017, November). Frictional stabil-
 412 ity and earthquake triggering during fluid pressure stimulation of an ex-
 413 perimental fault. *Earth and Planetary Science Letters*, 477, 84-96. doi:
 414 10.1016/j.epsl.2017.08.009
- 415 Segall, P., & Rice, J. R. (1995). Dilatancy, compaction, and slip instability of a
 416 fluid-infiltrated fault. *Journal of Geophysical Research: Solid Earth*, 100(B11),
 417 22155-22171. doi: 10.1029/95JB02403
- 418 Tordesillas, A. (2007). Force chain buckling, unjamming transitions and shear band-
 419 ing in dense granular assemblies. *Philosophical Magazine*, 87(32), 4987-5016.
 420 doi: 10.1080/14786430701594848

- 421 Van Den Ende, M. A., Marketos, G., Niemeijer, A., & Spiers, C. (2018). Investigat-
422 ing compaction by intergranular pressure solution using the discrete element
423 method. *Journal of Geophysical Research: Solid Earth*, *123*(1), 107-124. doi:
424 10.1002/2017JB014440
- 425 Yang, Z., & Juanes, R. (2018, Feb). Two sides of a fault: Grain-scale analysis of
426 pore pressure control on fault slip. *Physical Review E*, *97*, 022906. doi: 10
427 .1103/PhysRevE.97.022906